nature COMMUNICATIONS

ARTICLE

https://doi.org/10.1038/s41467-019-10108-0 OPEN

Local membrane charge regulates β_2 adrenergic receptor coupling to G_{i3}

M.J. Strohman[1], S. Maeda[1], D. Hilger[1], M. Masureel[1], Y. Du[1] & B.K. Kobilka[1]

The β_2 adrenergic receptor (β_2AR) signals through both G_s and G_i in cardiac myocytes, and the G_i pathway counteracts the G_s pathway. However, G_i coupling is much less efficient than G_s coupling in most cell-based and biochemical assays, making it difficult to study β_2AR—G_i interactions. Here we investigate the role of phospholipid composition on G_s and G_i coupling. While negatively charged phospholipids are known to enhance agonist affinity and stabilize an active state of the β_2AR, we find that they impair coupling to G_{i3} and facilitate coupling to G_s. Positively charged Ca^{2+} and Mg^{2+}, known to interact with the negative charge on phospholipids, facilitates G_{i3} coupling. Mutational analysis suggests that Ca^{2+} coordinates an interaction between phospholipid and the negatively charged EDGE motif on the amino terminal helix of G_{i3}. Taken together, our observations suggest that local membrane charge modulates the interaction between β_2AR and competing G protein subtypes.

[1] Department of Molecular and Cellular Physiology, Stanford University School of Medicine, Beckman Center Room B157, 279 Campus Drive, Stanford, CA 94305, USA. Correspondence and requests for materials should be addressed to B.K.K. (email: kobilka@stanford.edu)

A third of all FDA-approved pharmaceutical drugs function by modulating the activity of G-protein-coupled receptors (GPCRs)[1], a large receptor superfamily. GPCRs catalyze the activation of heterotrimeric G proteins, which in turn initiate a multitude of signaling cascades that alter cellular function.

The β_2 adrenergic receptor (β_2AR) is a prototypical GPCR that mediates the fight-or-flight response. β_2AR signals through both G_s and G_i, and the dual G protein selectivity of β_2AR is best characterized in heart muscle (cardiac myocytes). In healthy neonatal cardiac myocytes, epinephrine-stimulated β_2AR immediately activates G_s, increasing contraction rate, but after 10−15 min β_2AR signals predominantly through G_i [2], which decreases the contraction rate. In cardiac myocytes, β_2AR couples to both G_{i2} and G_{i3}[3]. Of interest, G_i activation is impaired if β_2AR internalization is blocked[4]. Also, G_i does not interact with a modified β_2AR that internalizes but does not recycle to the plasma membrane[5], or with WT β_2AR that internalizes but is pharmacologically blocked from recycling[6]. Taken together, these observations demonstrate that β_2AR−G_i interaction is regulated temporally and perhaps spatially.

During heart failure, a condition of chronic, progressive cardiac insufficiency, the G_i pathway counteracts some negative consequences of chronic G_s activation that exacerbate heart failure, namely apoptosis and structural and functional remodeling[7–9]. However, G_i activation reduces contractility, which can be problematic in certain models of heart failure[10]. More precise regulation of G_s and G_i activation is a therapeutic aim[9].

While β_2AR signals through both G_s and G_i, the mechanism that initiates the G_s-to-G_i switch in the healthy heart is not fully understood. Multiple biochemical mechanisms may play a role. PKA phosphorylation of β_2AR has been reported to increase G_{i1} coupling in vitro[11] and G_i coupling in HEK cells[12]; however, the G_{i1} subtype is not expressed in cardiac myocytes, and β_2AR−G_i coupling is PKA independent in these cells[2]. In addition, GRK2 phosphorylation of β_2AR has been suggested to increase G_i coupling[13], but other investigators have reported that dephosphorylation is critical for β_2AR recycling to the plasma membrane, and β_2AR−G_i interactions[6]. Therefore, the mechanisms that modulate β_2AR−G_i coupling remain unclear.

In vitro, negatively charged phospholipids stabilize an active conformation of the β_2AR and enhance its affinity for the catecholamine isoproterenol[14], but the effect of phospholipid charge on G protein coupling is unknown. Negatively charged lipids have previously been shown to facilitate β_1AR−G_s interaction[15], NTS1−G_q[16] interaction, CB_2−G protein interaction[17], and rhodopsin−G_t[18] interaction. In cardiac myocytes, β_2AR activates G_s in T-tubules[19], deep evaginations of the plasma membrane enriched in L-type calcium channels and negatively charged phospholipids[20]. β_2AR activation of G_i may also occur in T-tubules, after internalization and recycling. However, trafficking events may alter the composition of phospholipids surrounding the β_2AR. In addition, the β_2AR−G_s signaling that occurs prior to β_2AR−G_i signaling greatly increases the Ca^{2+} concentration near T-tubules[21], which may alter the charge properties of the T-tubule lipids[22].

Here we examine the effect of phospholipid charge on β_2AR interactions with G_s and G_{i3}. We find that negatively charged lipids enhance β_2AR interaction with G_s and impair interaction with G_{i3}. Further, Ca^{2+} and Mg^{2+} facilitate β_2AR−G_{i3} interaction in negatively charged lipids. Our observations suggest that local membrane charge, tuned by intracellular cations, modulates β_2AR interaction with G_{i3}.

Results

Monitoring G protein coupling by fluorescence spectroscopy. Epinephrine activates β_2AR by partially stabilizing the conformation recognized by the G protein. This conformation is fully stabilized upon G protein coupling[23–25]. A feature of the G-protein-coupled conformation of β_2AR is a 14 angstrom outward displacement of the cytoplasmic end of β_2AR transmembrane segment 6 (TM6) (Fig. 1a). This conformation can be detected by fluorescence spectroscopy, using a modified β_2AR labeled at the cytoplasmic end of TM6 with an environmentally sensitive fluorophore, monobromobimane (mB−β_2AR, see Methods and ref. [26]). Outward movement of TM6 affects the environmental polarity of mB, going from the hydrophobic receptor core to the solvent, decreasing the intensity of mB and increasing the wavelength where emission intensity is greatest (λ_{max}), from ~447 to ~468 nm (Fig. 1a). We monitor λ_{max} to detect G protein coupling, as λ_{max} increases with coupling (Supplementary Fig. 1).

Negatively charged lipids inhibit β_2AR-G_i coupling. In the presence of epinephrine, we observe a change in intensity and λ_{max} of mB−β_2AR following the addition of G_s in a detergent mixture containing *n*-dodecyl-β-D-maltopyranoside (DDM) and cholesteryl hemisuccinate (CHS) that is commonly used for biochemical study of GPCR/G protein complexes (Fig. 1a). In contrast, the coupling efficiency of mB−β_2AR−G_{i3} was relatively weak (Fig. 1a). Next, we compared the coupling efficiency of mB−β_2AR−G_i in DDM + CHS mixtures with different phospholipids incorporated (Fig. 1b–d). While we were unable to detect interactions of mB−β_2AR with G_{i1}, G_{i2} or G_{i3} in the presence of negatively charged lipids phosphatidylserine (POPS) and phosphatidylglycerol (POPG), we observed a weak interaction with G_{i1} and G_{i3} in neutral lipids phosphatidylethanolamine (POPE) and phosphatidylcholine (POPC) (Fig. 1c, d—G_{i1} and G_{i3} with epinephrine stabilizes more mB−β_2AR in the active conformation than epinephrine alone). This result suggested that negatively charged lipids may repel G_{i1} and G_{i3} interaction with β_2AR.

Indeed, we observed that negatively charged CHS decreased mB-β_2AR-G_{i3} coupling (Fig. 1e), supporting our hypothesis that negatively charged lipids inhibit coupling. Since CHS is a nonphysiologic cholesterol analog, we omitted negatively charged CHS in subsequent experiments in order to isolate the effect of phospholipid charge on mB−β_2AR−G_i interactions.

Given reports that PKA phosphorylation of β_2AR increases β_2AR−G_i interaction in vitro[11], we also tested the effect of PKA phosphorylation, but no enhancement of mB−β_2AR interaction with G_{i1}, G_{i2}, or G_{i3} was observed (Supplementary Fig. 2), suggesting that phosphorylation does not potentiate β_2AR−G_i interaction under our experimental conditions, and that other mechanisms may enhance β_2AR−G_i interaction.

In contrast to G_{i1} and G_{i3}, we were unable to detect coupling to G_{i2} in any of the lipid-detergent mixtures (Fig. 1c), suggesting that the interaction is low affinity. Of interest, G_{i1} and G_{i3} share higher sequence identity than either subtype shares with G_{i2}. To confirm the lack of coupling to G_{i2} observed by fluorescence analysis, we examined β_2AR-stimulated G protein turnover of GTP in net neutral DDM + POPC for G_{i2} and G_{i3} (Supplementary Fig. 3). As expected from our fluorescence studies, we observed robust β_2AR-induced GTP turnover for G_{i3}, but only weak β_2AR-induced GTP turnover for G_{i2}. In contrast we observed strong coupling of G_{i2} to purified neurotensin receptor, indicating that the G_{i2} protein was functional. While both G_{i2} and G_{i3} couple to β_2AR in cardiac myocytes[3], the coupling efficiency using purified components is substantially different (see Discussion). We therefore focused on β_2AR−G_{i3} coupling in further studies.

Next we examined how the lipid environment affects β_2AR activation of G_{i3}. In the presence of epinephrine, significantly more β_2AR-induced GTP turnover was detected in DDM micelles

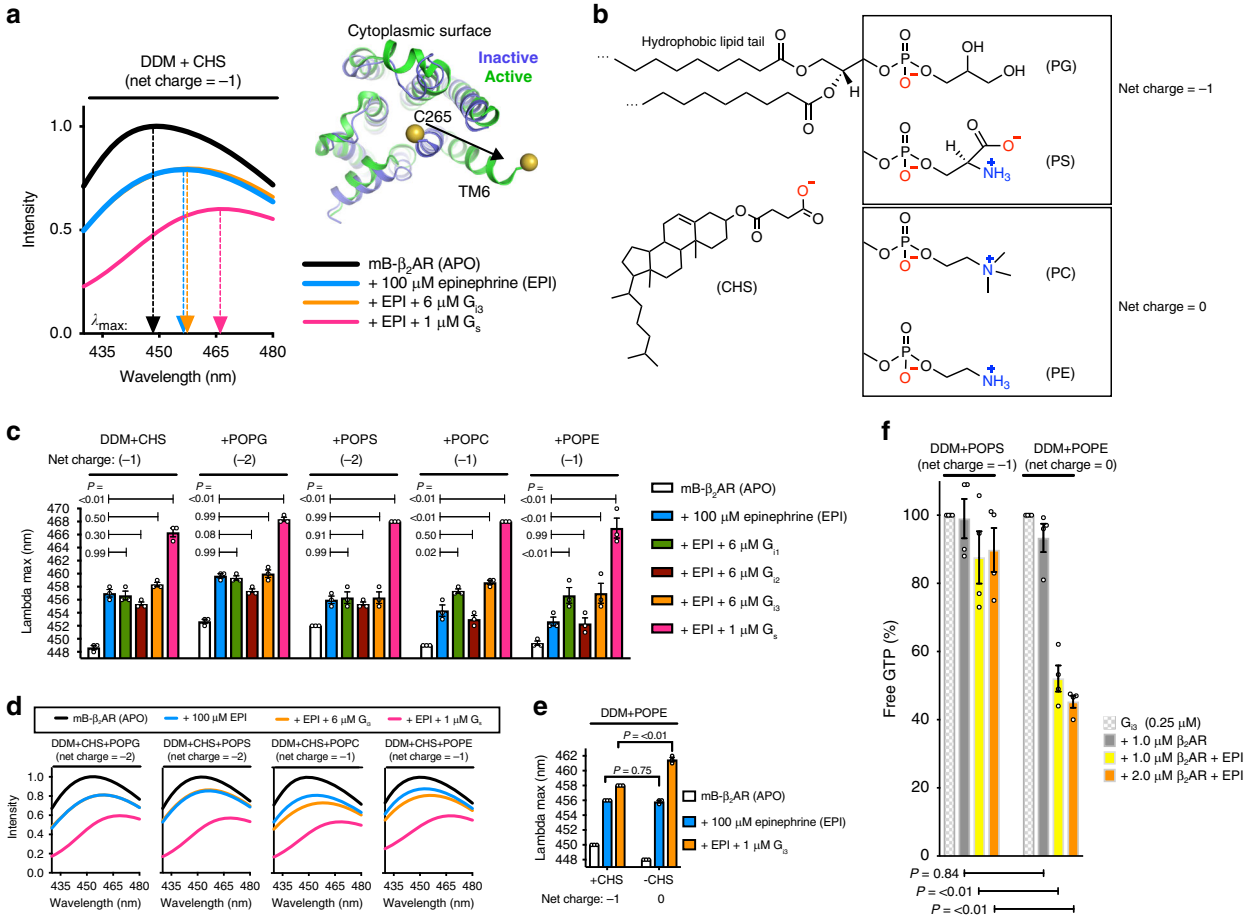

Fig. 1 Negatively charged lipids inhibit β_2AR–G_i coupling in detergent. **a** mB–β_2AR emission spectra in DDM + CHS micelles (5:1 DDM:CHS mole ratio) in the absence of epinephrine (APO) and in the presence of epinephrine, ± G protein (G_s or G_{i3}). Arrows point to the lambda max value, i.e. the wavelength where mB emission intensity is greatest. Inset shows how G_s coupling alters the structure of mB–β_2AR, highlighting the change in position of monobromobimane (mB) at C265 of transmembrane 6 (TM6) (Inactive: PDB 5JQH[74]; Active: PDB 3SN6[69]). **b** Structures of CHS and phospholipids, with net charge indicated. **c** Effect of phospholipid on mB–β_2AR interaction with G protein (G_{i1}, G_{i2}, G_{i3}, and G_s), read out as an increase in lambda max. Interaction was assessed in the absence of lipid (5:1 DDM:CHS mole ratio) and in the presence of POPG, POPS, POPC, or POPE (5:1:1 DDM:CHS:Lipid mole ratio). Multiplicity adjusted *P* values were computed by two-way ANOVA followed by Dunnett's post hoc test between indicated groups. **d** Selected mB–β_2AR emission spectra from panel (**c**). **e** Effect of CHS on mB–β_2AR interaction with 1 μM G_{i3}. Interaction was assessed in the presence of CHS (5:1:1 DDM:POPE:CHS mole ratio) or in the absence of CHS (5:1 DDM:POPE mole ratio). Multiplicity adjusted *P* values were computed by two-way ANOVA followed by Sidak's post hoc test between indicated groups. **a**–**e** mB–β_2AR concentration is 300 nM. Data are mean of three independent experiments. **f** β_2AR-induced GTP turnover for G_{i3} (± 200 μM epinephrine, EPI) in DDM + POPS (5:1 DDM:POPS mole ratio) and in DDM + POPE (5:1 DDM:POPE mole ratio). Free GTP was assayed after 12 min. Luminescence signals were normalized relative to the condition with G_{i3} alone (see Supplementary Fig. 4). Data are mean ± s.e.m. of four independent experiments. Multiplicity adjusted *P* values were computed by two-way ANOVA followed by Sidak's post hoc test between indicated groups. Source data are provided in the Source Data File

containing POPE (net neutral lipid) than in DDM micelles containing POPS (net negative) (Fig. 1f). This effect on β_2AR-mediated turnover was significant, even though the lipid:DDM mole ratio was only 1:5. POPE did not increase basal GTP turnover by G_{i3} in the absence of β_2AR (Supplementary Fig. 4). Taken together, these results indicate that the charge property of phospholipids regulates G_i activation by β_2AR.

Ca^{2+} facilitates G_{i3} coupling in negatively charged lipids. Ca^{2+}, a ubiquitous second messenger, plays an important role in cardiac myocytes; Ca^{2+} waves, magnified by G_s activation, drive the cardiac myocyte contraction machinery. Recently Ca^{2+} was reported to regulate T-cell receptor activation by modulating the charge property of lipids[27]. Given that Ca^{2+} interaction with negative charge on phospholipids neutralizes the charge, we tested whether Ca^{2+} improves mB–β_2AR–G_{i3} coupling efficiency in negatively charged DDM + POPS. Indeed, Ca^{2+} improved coupling efficiency in DDM + POPS micelles (Fig. 2a), and this effect required lipid (Fig. 2b). Moreover, Ca^{2+} had little effect on mB–β_2AR–G_s interaction, implicating differences in G_s and G_{i3} surface charge.

Ca^{2+} interacts with the amino terminal helix of G_{i3}. Next, we sought to determine the mechanism by which Ca^{2+}–POPS interactions increase mB–β_2AR coupling to G_{i3} but not to G_s. Given that the amino terminal helix (αN) of G protein is adjacent to the membrane when coupled to the β_2AR[25], and polybasic residues on G_s αN are known to facilitate membrane interaction[28], we looked for a possible selectivity determinant within αN. Since αN of G_s and G_i are differentially charged (Fig. 3a), we first

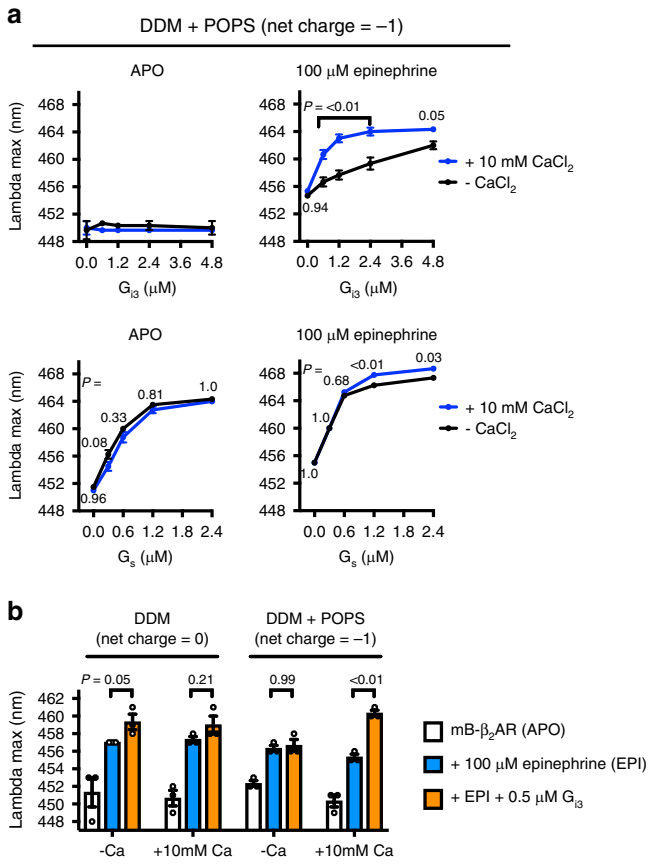

Fig. 2 Ca^{2+} facilitates G_{i3} coupling in negatively charged phosphatidylserine. **a** The effect of 10 mM $CaCl_2$ on mB−β_2AR−G protein interaction (G_{i3} and G_s) was examined in micelles containing 5:1 DDM: POPS (mole ratio). Data were collected in the absence (APO) and presence (100 μM) of epinephrine. mB−β_2AR concentration is 250 nM. Data are mean ± s.e.m. of three independent experiments. Multiplicity adjusted *P* values were computed by two-way ANOVA followed by Sidak's post hoc test between $CaCl_2$ conditions. **b** The effect of 10 mM $CaCl_2$ on mB−β_2AR−G_{i3} interaction in DDM micelles ± POPS (i.e. DDM alone vs. 2.5:1 DDM: POPS mole ratio). mB−β_2AR concentration is 250 nM. Data are mean ± s.e.m. of three independent experiments. Multiplicity adjusted *P* values were computed by three-way ANOVA followed by Sidak's post hoc test between indicated groups. Source data are provided in the Source Data File

replaced αN of G_s with αN of G_{i3}, creating a G_{i3}-G_s chimera (Fig. 3b).

While Ca^{2+} does not promote mB−β_2AR coupling to WT G_s (Fig. 3b), it did promote mB−β_2AR coupling to the G_{i3}-G_s chimera (Fig. 3b). Next, we compared the membrane-facing charge of G_s WT αN and G_{i3} WT αN. Structural analysis revealed that charge differed at the C terminal end of αN: G_i harbors a negatively charged motif (EDGE) at the position where G_s harbors a positively charged motif (KDKQ) (Fig. 3a). To examine whether this motif dictates a differential response to Ca^{2+}, we constructed a G_s mutant (G_s-neg.) containing the negatively charged motif of G_{i3} (KDKQ → EDGE). Ca^{2+} increased mB−β_2AR interaction with this mutant (Fig. 3b), suggesting the EDGE motif is responsible for the effect of Ca^{2+} on G_{i3} αN. Taken together, our results imply that Ca^{2+} coordinates an interaction between the negatively charged EDGE motif on αN of G_{i3} and the headgroup of POPS. In the absence of Ca^{2+}, like-charge repulsion decreases mB-β_2AR coupling to G_{i3}.

We also constructed a G_{i3} mutant (G_{i3}-pos.) containing the positively charged motif of G_s (EDGE → KDKQ). The mutations only partially removed the effect of Ca^{2+} (Fig. 3b), indicating the effect of Ca^{2+} on G_{i3} extends beyond an effect on αN (see Discussion).

Bilayer charge differentially affects G_s and G_{i3} coupling. Owing to their geometry and charge, phospholipids might induce changes in the size and shape of micelle assemblies which could also influence mB−β_2AR−G protein interaction[29,30]. To examine the effects of phospholipids in a more native environment, and to restrict the size and shape of lipid ensembles, helping us isolate the effect of membrane charge, we reconstituted mB−β_2AR into nanodisc bilayers and purified the nanodiscs to homogeneity using size-exclusion chromatography (Supplementary Fig. 5).

First, we compared the influence of lipid composition in the absence of Ca^{2+}. Negatively charged bilayers (DOPG and DOPS bilayers), previously reported to increase agonist affinity[14], expectedly red-shifted the emission spectra of unliganded mB−β_2AR, suggesting these lipids stabilize an active conformation. Additionally, unliganded mB-β_2AR and G_s could fully couple in negatively charged bilayers but not in neutral bilayers (Fig. 4), suggesting negatively charged lipids might facilitate signaling through G_s. In contrast, negatively charged lipids (especially DOPS bilayers) decreased G_{i3} coupling to epinephrine-activated mB−β_2AR (Fig. 4).

In fact, in negatively charged bilayers without epinephrine, G_{i3} unexpectedly blue-shifted the emission spectra of mB−β_2AR. While this may indicate that G_{i3} stabilizes the β_2AR in an inactive conformation in negatively charged lipids, it may represent a nonspecific interaction of inactive G_{i3} with the β_2AR or the lipid bilayer.

Cations promote G_{i3} coupling in negatively charged bilayers. Next we examined the effect of Ca^{2+} and Mg^{2+}. In the absence of G_{i3}, both Ca^{2+} and Mg^{2+} reversed the active-state stabilizing effect of negatively charged DOPS and DOPG bilayers (Fig. 5a). Despite this, Ca^{2+} and Mg^{2+} increased mB-β_2AR coupling to G_{i3} in negatively charged DOPS bilayers, but only Ca^{2+} was efficacious at concentrations below 1 mM (Fig. 5a). Ca^{2+} similarly affected mB−β_2AR−G_{i3} interaction in negatively charged DOPG bilayers (Fig. 5a), but the magnitude of the effect in DOPG bilayers was less than observed in DOPS bilayers due to the higher baseline effect of DOPG on β_2AR conformation.

We also compared the effect of Ca^{2+} on mB−β_2AR interactions with G protein subtypes (G_s versus G_{i3}) in DOPS bilayers. As observed in micelles, Ca^{2+} increased mB−β_2AR coupling to G_{i3} but not to G_s (Fig. 5b). Ca^{2+} also improved mB−β_2AR−G_{i3} coupling efficiency in negatively charged DOPG bilayers (Fig. 5c). However, incorporating Ca^{2+} did not enable detection of mB−β_2AR interaction with the G_{i2} subtype of G_i (Fig. 5d, see Discussion).

While Ca^{2+} interacts with net negative PS and PG with relatively high affinity, it also interacts with the negatively charged phosphate group on net neutral PC[31] and PE lipids[31,32]. In neutral DOPE and DOPC bilayers (Fig. 5c and Supplementary Fig. 6), Ca^{2+} only slightly enhanced mB−β_2AR−G_{i3} interaction, which could be attributable to weaker Ca^{2+}/DOPE and Ca^{2+}/DOPC interactions that have been reported. Taken together, our observations provide biochemical evidence that local membrane charge can regulate β_2AR−G protein interaction.

Discussion

We observed that local membrane charge regulates β_2AR−G protein interaction. Negatively charged membrane promotes β_2AR−G_s coupling and suppresses β_2AR−G_{i3} coupling. However, G_s bias is reduced in neutral membrane and in negatively charged

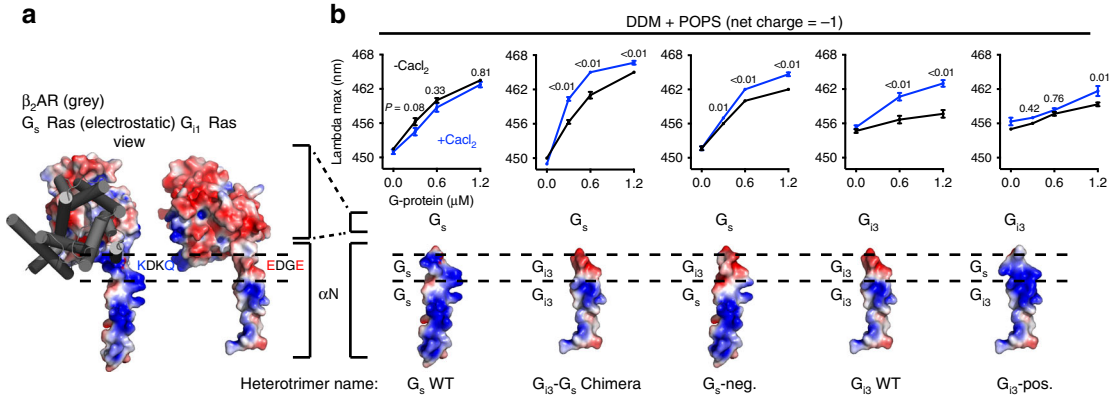

Fig. 3 Ca^{2+} interacts with the amino terminal helix of G_{i3}. **a** Membrane-facing surfaces of G_s and G_{i1} Ras domains, with β_2AR shown in gray. The membrane-facing surface of G_{i1} was modeled by superimposing the Ras domain of G_{i1} (PDB: 1GP2[70]) onto the structure of G_s in complex with β_2AR (PDB: 3SN6[69]). Red and blue signify negative and positive charge on G protein, respectively. Dashed lines highlight the region in αN where charge differs: The sequence is KDKQ in WT G_s vs. EDGE in WT G_{i1} (and in G_{i2}, G_{i3}). **b** mB−β_2AR−G protein dose−response curves ± 10 mM $CaCl_2$. Data were generated with the G protein depicted below the curves: mutations were made in αN and corresponding electrostatic models are shown. Epinephrine was not included in experiments titrating G_s WT, G_{i3}-G_s Chimera, or G_s-neg. to enhance the effect of $CaCl_2$. Epinephrine (100 μM) was included in experiments titrating G_{i3} WT and G_{i3}-pos. mB−β_2AR concentration is 250 nM. Data are mean ± s.e.m. of three independent experiments. Multiplicity adjusted *P* values were computed by two-way ANOVA followed by Sidak's post hoc test between $CaCl_2$ conditions. Source data are provided in the Source Data File

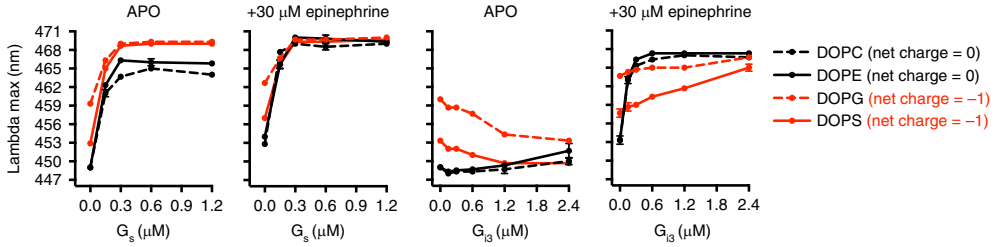

Fig. 4 Bilayer charge differentially affects G_s and G_{i3} coupling. The effect of G_s (left) and G_{i3} (right) concentration on mB−β_2AR fluorescence was examined in nanodisc bilayers of varying phospholipid composition (DOPC, DOPE, DOPG, DOPS). Epinephrine was omitted (APO) or included (30 μM). Interaction with G protein is read out as an increase in lambda max. The net charge of the phospholipid is indicated in parentheses. mB−β_2AR concentration is 100 nM; maximum stoichiometry is 12:1 (for G_s) and 24:1 (for G_{i3}). Data are mean ± s.e.m. of three independent experiments. Source data are provided in the Source Data File

membrane in the presence of divalent cations (see model in Fig. 6).

We have begun to explore the mechanism by which Ca^{2+} increases mB−β_2AR coupling to G_{i3} in phospholipids. The effect of Ca^{2+} was largely dependent on charged groups on G_{i3}, indicating Ca^{2+} doesn't simply affect membrane structure. Although G proteins are membrane tethered via lipidation, the lipid anchor of G_{i3} is not sufficient for optimal interaction with β_2AR in negatively charged bilayers, possibly due to repulsion of the carboxyl terminal end of the αN helix. We propose that Ca^{2+} helps orient the carboxyl terminal end of the αN helix of G_{i3} near the membrane, thereby facilitating β_2AR−G_{i3} interactions. More specifically, we propose that Ca^{2+} facilitates the interaction of lipid with the negatively charged EDGE motif on the αN helix of G_{i3}. Ca^{2+} may coordinate a like-charge interaction between the carboxylate groups on the G_{i3} EDGE motif and the phosphate group present on all lipids. In addition, Ca^{2+} may especially stabilize EDGE interaction with PS lipids by coordinating a like-charge interaction between the carboxylate groups on the G_{i3} EDGE motif and the carboxylate group on PS (not present on PG) (refer to structures in Fig. 1b), or Ca^{2+} might coordinate an intramolecular interaction between the phosphate group and the carboxylate group on PS, freeing the amino group (NH_3^+) on PS to interact with the carboxylate groups on G_{i3}.

We have previously shown that negatively charged lipids, particularly PG, stabilize the β_2AR in an active-like conformation as revealed by changes in mB−β_2AR fluorescence and an increased affinity for agonists[14]. These effects are likely due to interactions between the lipids and positively charged amino acids on the β_2AR. Here we observed that the effect of DOPG and DOPS on mB-β_2AR can be reversed by both Ca^{2+} and Mg^{2+} (Fig. 5a). Yet, these divalent cations do not appear to reduce coupling to G_s.

β_2AR signals from caveolin-rich rafts[33,34] within T-tubules[19]. While β_2AR preferentially interacts with PG in insect cell membrane[14], the phospholipid composition immediately adjacent to β_2AR in T-tubules, and how it changes during β_2AR trafficking, is currently unknown. Net-neutral PC and PE are the major phospholipids in T-tubules[35–37]. However, negatively charged PS is enriched in T-tubules relative to other membrane fractions (7.5−12.3% of total phospholipid)[35–39]. While cytosolic Ca^{2+} concentrations are typically less than 1 mM[40], concentrations of Ca^{2+} in the mM range may be observed in cardiac myocytes.

Investigators have long speculated about the functional role of Ca^{2+} in the cleft between the T-tubule membrane (where β_2AR is localized) and the juxtaposed sarcoplasmic reticulum (SR)[21,22,41]. During each action potential, extracellular Ca^{2+} flows into the cleft through L-type Ca^{2+} channels (LTCCs) on the plasma membrane and through ryanodine receptors (RyRs) on the

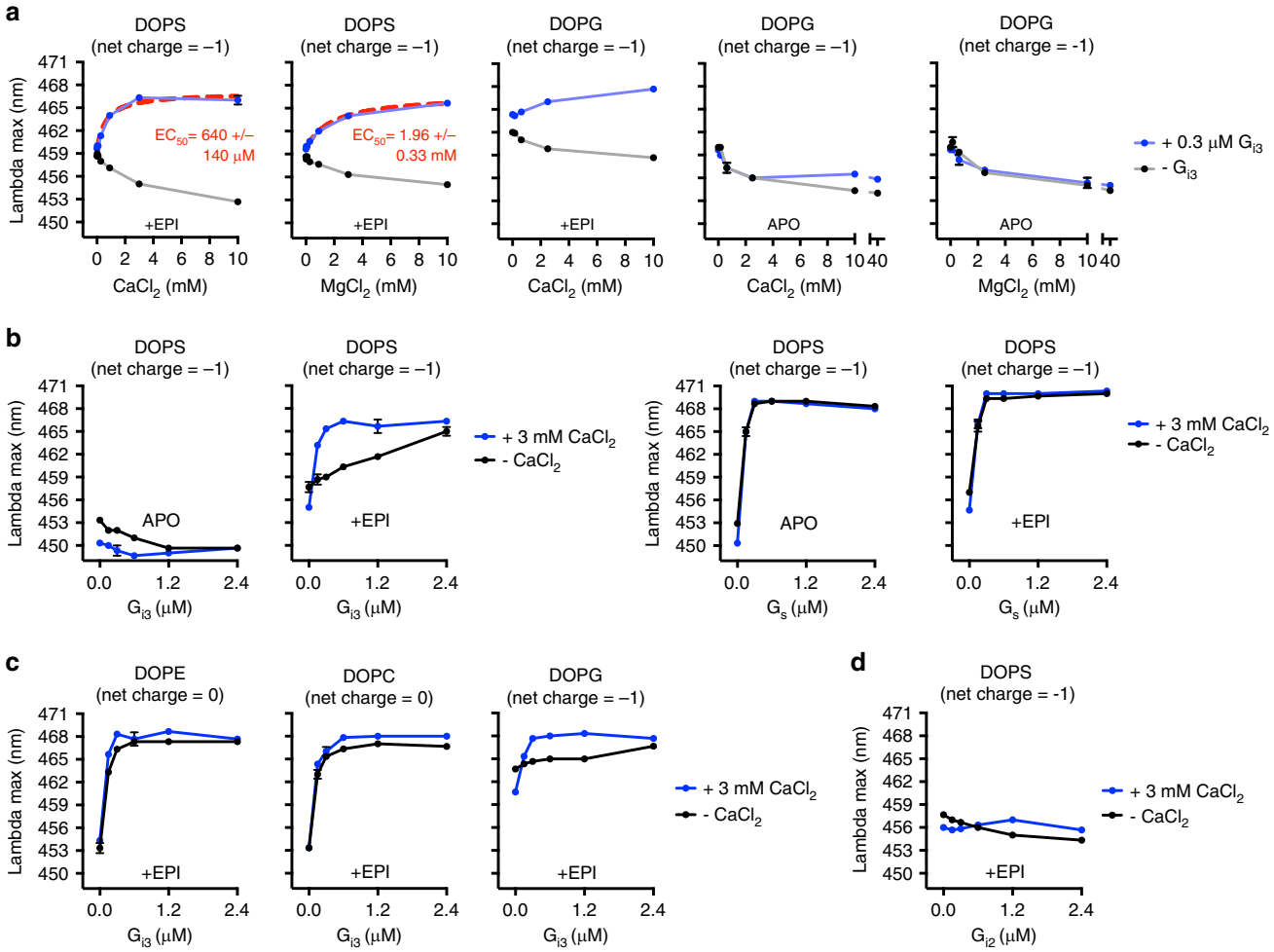

Fig. 5 Ca^{2+} and Mg^{2+} facilitate G_{i3} coupling in negatively charged bilayers **a** The effect of $CaCl_2$ and $MgCl_2$ concentration on mB–β_2AR fluorescence in DOPS and DOPG nanodisc bilayers was examined in the presence and absence of G_{i3}. Epinephrine was included (30 μM) or omitted (APO). EC_{50} is mean ± s.e.m. **b** The effect of G protein concentration (G_{i3} and G_s) on mB–β_2AR fluorescence ± 3 mM $CaCl_2$ was examined in DOPS nanodiscs in the absence (APO) and in the presence (EPI) of epinephrine (30 μM). **c** The effect of G_{i3} on mB–β_2AR fluorescence ± 3 mM $CaCl_2$ was examined in DOPE, DOPC, and DOPG nanodisc bilayers in the presence of 30 μM epinephrine (EPI). **d** The effect of G_{i2} concentration on mB–β_2AR fluorescence ± 3 mM $CaCl_2$ was examined in DOPS nanodisc bilayers in the presence of 30 μM epinephrine (EPI). **a**–**d** mB–β_2AR concentration is 100 nM. The net charge of the phospholipid molecule is indicated in parentheses. Data are mean ± s.e.m. of three independent experiments. Source data are provided in the Source Data File

sarcoplasmic reticulum[40]. Cleft Ca^{2+} concentrations spark to >100 μM in the absence of epinephrine and >1 mM[42,43] following epinephrine stimulation, a consequence of G_s activation. Computational models show that negatively charged phospholipids buffer approximately half the Ca^{2+} released into the cleft[42], and experiments have shown that 80% of inner-leaflet bound Ca^{2+} is bound to negatively charged phospholipids[44]. Additionally, biochemical investigations show that Ca^{2+} can cluster negatively charged PS[45] and PIP_2[46,47] lipids.

β_1AR and β_2AR signaling through G_s alters calcium handling in the cardiac myocyte, and increases the magnitude of Ca^{2+} currents and Ca^{2+} transients, which stimulate cardiac contraction[40,48]. However, elevated Ca^{2+} concentrations also activate the Ca^{2+}/calmodulin-dependent protein kinase II (CaMKII), which promotes apoptosis, and is implicated in structural remodeling that ultimately results in cardiac dysfunction[9,49–52]. Elevated Ca^{2+} also activates calcineurin, which exacerbates pathological hypertrophy[21]. For these reasons, β_1AR-selective (and nonselective) beta blockers have proven to be efficacious medicines for treatment of heart failure[53]. However, β_2AR, owing to its dual G_s/G_i selectivity, is functionally distinct from the strictly G_s-coupled β_1AR, and several lines of evidence suggest β_2AR–G_i signaling functions to keep G_s signaling in check via negative feedback: β_2AR–G_i signaling occurs minutes after β_1AR–G_s and β_2AR–G_s signaling[2], β_2AR–G_i signaling suppresses changes in calcium handling[48,54], and β_2AR–G_i signaling is antiapoptotic[7,8]. While the mechanism that triggers β_2AR–G_i signaling is unknown, our biochemical observations suggest elevated Ca^{2+} concentrations could trigger β_2AR coupling to G_{i3}. It is notable that overexpression of the Ca^{2+}/sodium exchanger facilitates β_2AR–G_i suppression of β_1AR–G_s signaling[55], and overexpression has been cited to increase the inward LTCC Ca^{2+} current[56].

It is also notable that intracellular Ca^{2+} [57,58] and Mg^{2+} [58] concentrations rise during ischemia and rise even higher during reperfusion. Whether the rising concentrations facilitate β_2AR-G_i signaling is unknown. However, β_2AR–G_i signaling can reduce the extent of cardiac necrosis caused by ischemia and reperfusion[59].

We were surprised that we did not observe mB–β_2AR coupling to G_{i2} under conditions where we observed coupling to G_{i1} and G_{i3} (Fig. 1c, Supplementary Fig. 3). Although G_{i2} contains the αN

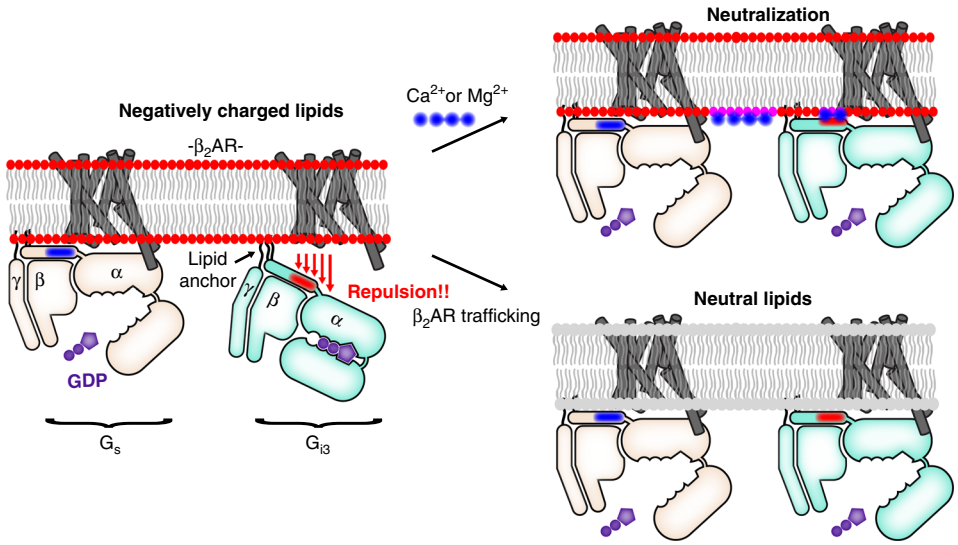

Fig. 6 Membrane charge is a tunable modulator of β_2AR−G protein interaction. Models depict epinephrine-bound β_2AR. Left: In negatively charged lipids, β_2AR−G_s coupling is efficient, but β_2AR−G_{i3} coupling is relatively inefficient, in part because β_2AR−G_{i3} attraction is countered by membrane-G_{i3} repulsion. Specifically, negatively charged lipids repel the negatively charged EDGE motif found on the amino terminal helix of G_{i3} (shown in red), a region that is positively charged in G_s (shown in blue). Right: Two mechanisms that neutralize membrane charge facilitate β_2AR coupling to G_{i3}. These mechanisms may play a role in G_s-to-G_i switching in cardiac myocytes. Top right: Ca^{2+} and Mg^{2+} stabilize a like-charge interaction between the membrane and the EDGE motif. (Note that the effect of Ca^{2+} and Mg^{2+} may extend beyond an effect on αN positioning.) Bottom right: Epinephrine-stimulated β_2AR traffics to membrane without negatively charged lipids

EDGE motif, we did not observe mB−β_2AR−G_{i2} interaction in the presence of Ca^{2+} (Fig. 5d). While the sequences of $G\alpha_{i1}$ and $G\alpha_{i3}$ are 94% identical, $G\alpha_{i2}$ shares less sequence identity with $G\alpha_{i1}$ and $G\alpha_{i3}$, 88% and 86%, respectively. Supplementary Fig. 7 shows the location of the amino acid differences in G_{i2} relative to both G_{i1} and G_{i3} using the recent cryo-electron microscopy structure of the adenosine A1-G_{i2} complex (PDB: 6D9H[60]). It can be seen that these amino acids do not appear to interact directly with the receptor in the nucleotide-free complex. However, these amino acids may form weak interactions with the poorly ordered intracellular loop 3 that is not observed in the structure, or may interact with other domains of the receptor during complex formation. Previous studies provide evidence for at least one transient intermediate state in formation of the β_2AR−G_s complex[61]. Both G_{i2} and G_{i3} couple to β_2AR in cardiac myocytes[3]. However, during heart failure, G_{i2} expression is commonly upregulated[62–64]. In contrast, G_{i3} upregulation, while reported[65], is less commonly observed. How selective G_{i2} upregulation influences β_2AR−G_i signaling is not fully understood. Signaling through G_{i2} and G_{i3} could play different roles in cardiac physiology. It is possible that β_2AR coupling to G_{i3} plays a role in preventing myocyte damage during transient ischemia or prolonged periods of adrenergic stimulation, such as during exercise. Both of these conditions would be associated with elevated cytosolic Ca^{2+}. In contrast, β_2AR coupling to G_{i2} may play a more prominent role in the failing heart.

G proteins are a large superfamily, grouped into four subfamilies (G_s, $G_{i/o}$, $G_{q/11}$, $G_{12/13}$) encoded by 16 different genes[66]. Each subfamily activates distinct signaling pathways, and functional effects are cell-type specific. Most GPCRs can signal through more than one G protein subfamily, and ongoing research attempts to identify mechanisms that regulate G protein selectivity within a cell[66]. Whether local membrane charge affects G_i interaction with other G_i-coupled GPCRs is not currently known. In cardiac myocytes, β_2AR signals from a PS-enriched, Ca^{2+}-enriched microenvironment, which highlights the potential relevance of our biochemical observations. Additionally, the observation that Ca^{2+} sensing receptor (CaSR) switches from G_q to G_i after cytosolic Ca^{2+} increases[67] is also potentially relevant to our findings. However, knowledge that Ca^{2+} facilitates G_i interaction with membrane is not sufficient to predict how Ca^{2+} might affect G_i interaction with other receptors.

In conclusion, we show that local membrane charge differentially modulates β_2AR interaction with competing G protein subtypes (G_s and G_i). This discovery expands our knowledge of mechanisms that regulate the G protein coupling selectivity of GPCRs.

Methods

G protein expression and purification. All G proteins were human heterotrimeric G proteins (Gα, $G\beta_1$, $G\gamma_2$). The $G\beta_1$ subunit contained an N-terminal 6xHis tag followed by a rhinovirus 3C protease site used for purification[61]. $G\alpha_s$ was the short splice variant. The G_{i3}-G_s chimera was created starting with $G\alpha_s$, replacing residues 1−38 (the αN helix) with the equivalent region of $G\alpha_{i3}$ (residues 1−31 of $G\alpha_{i3}$)[68]. G_s-neg. was a G_s mutant with residues 32−35 of $G\alpha_s$ (KDKQ) replaced with the equivalent region in $G\alpha_{i3}$ (EDGE). G_{i3}-pos. was a G_{i3} mutant with residues 25−28 of $G\alpha_{i3}$ (EDGE) replaced with the equivalent region in $G\alpha_s$ (KDKQ). G protein was expressed in *Tni* insect cells (Expression Systems Cat. 94-002S) using two recombinant baculoviruses, a virus encoding Gα and a separate virus encoding both the $G\beta_1$ and $G\gamma_2$ subunits. Following infection, cells were incubated for 48 h at 27 °C, harvested by centrifugation, and suspended in lysis buffer (10 mM Tris (pH 7.5), 100 μM $MgCl_2$, 5 mM β-mercaptoethanol (BME), 10 μM GDP, and protease inhibitors). The membrane fraction was collected by centrifugation and solubilized using a Dounce homogenizer and buffer comprised of 20 mM HEPES (pH 7.4), 100 mM NaCl, 1% sodium cholate, 0.05% *n*-dodecyl-β-D-maltopyranoside (DDM), 5 mM $MgCl_2$, 5 mM BME, 10 μM GDP, and protease inhibitors. The soluble fraction was isolated by centrifugation, G protein was captured on Sepharose Fast Flow (GE Healthcare) charged with nickel, and gradually exchanged into SEC buffer (20 mM HEPES (pH 7.4), 100 mM NaCl, 0.05% DDM, 100 μM TCEP, 10 μM GDP, 1 mM $MgCl_2$). 3C protease was added to cleave G protein off the resin, and the G protein was dephosphorylated using calf intestinal alkaline phosphatase, antarctic phosphatase, and lambda protein phosphatase. Subsequently, G protein was isolated in SEC buffer using a Superdex 200 10/300 GL column (GE Healthcare). The main peak corresponding to heterotrimeric G protein was collected, concentrated, and frozen.

Receptor expression, purification, and labeling. The β_2AR construct was PN1[14], where human WT β_2AR (R16, Q27 variant) is modified to contain an N-terminal FLAG tag, a C-terminal rho-1D4 tag, a TEV protease cleavage site between V24 and T25, and a 3C protease cleavage site between G365 and Y366. Additionally, mutations were introduced to increase expression (M96T, M98T), to remove a glycosylation site (N187E) and to remove reactive cysteines (C378A, C406A). β_2AR

was expressed in *Sf*9 insect cells (Expression Systems Cat. 94-001S) using recombinant baculovirus and media supplemented with 1 μM alprenolol. Cells expressing β_2AR were harvested by centrifugation and suspended in lysis buffer (10 mM HEPES (pH 7.4), 1 mM EDTA, 1 μM alprenolol, and protease inhibitors). The membrane fraction was collected by centrifugation and solubilized using a Dounce homogenizer and buffer comprised of 20 mM HEPES (pH 7.4), 100 mM NaCl, 1% *n*-dodecyl-β-D-maltopyranoside (DDM), 0.03% CHS, 2 mM $MgCl_2$, 1 μM alprenolol, and protease inhibitors. The soluble fraction was isolated by centrifugation and anti-FLAG (ATCC HB-9259) affinity chromatography was used to purify β_2AR, remove alprenolol, and adjust detergent concentration (to 0.1% DDM, 0.01% CHS). Monobromobimane (mB, Thermo Fisher Scientific) labeling was then performed overnight with excess mB in the presence of 100 μM TCEP and the reaction was quenched with 5 mM L-cysteine before further purification. All β_2AR preparations were functionally purified by alprenolol-Sepharose affinity chromatography and washed on an anti-FLAG column to remove ligand. The eluted β_2AR was dialyzed in buffer comprised of 20 mM HEPES (pH 7.4), 100 mM NaCl, 0.1% DDM, and 0.02% CHS, concentrated, and dephosphorylated using lambda protein phosphatase. For experiments assessing phosphorylation, unphosphorylated β_2AR was phosphorylated with protein kinase A in the presence of 2 mM ATP. β_2AR was stored frozen. Phosphorylation was assessed using the Pro-Q Diamond Phosphoprotein Gel Stain (ThermoFisher Scientific), per the manufacturer's instructions. Stained acrylamide gels were scanned with a Typhoon 9410 Imager (GE Healthcare). Recombinant human NTSR1 (residues 20−418) contained an $A85^{1.54}L$ mutation to increase expression. NTSR1 was purified from *Sf*9 insect cells into buffer comprised of 20 mM HEPES (pH 7.5), 100 mM NaCl, 5% glycerol, 0.01% lauryl maltose neopentyl glycol (LMNG), 0.001% CHS, and 0.5 μM JMV 449, and stored frozen.

Ligands. (−) epinephrine was purchased from Sigma (purity > 99%). JMV 449 was purchased from Tocris (purity 97.6%).

Micelle composition. *n*-dodecyl-β-D-maltopyranoside (DDM), cholesteryl hemisuccinate (CHS), and 1-palmitoyl-2-oleoyl-sn-glycero-3-(PE,PC,PG,PS) lipids (Avanti Polar Lipids) were mixed in the indicated ratios and solubilized in chloroform. Chloroform was evaporated, and the films were re-suspended in 20 mM HEPES (pH 7.4), 100 mM NaCl.

Fluorescence spectroscopy. In experiments examining mB-β_2AR in micelles, mB−β_2AR was preincubated (30 min room temperature) in micelle stock prior to dilution with other reaction components. pH 7.4 HEPES buffer (containing 100 mM NaCl, ± ligand, ± $CaCl_2$ or $MgCl_2$) and G protein were sequentially included. Mixtures were incubated 2.5–3.0 h at room temperature. Final mB−β_2AR concentration was 100−300 nM. Emission spectra were read at 22 °C using a Fluorolog-3 spectrofluorometer (Horiba Jobin Yvon Inc.). (Bandpass = 4 nm; Excitation = 370 nm; Emission = 420−500 nm, collected in 1 nm increments). The raw S1c/R1c spectra were smoothed using Prism (GraphPad Software) ($n = 15$ neighbors, second-order polynomial). Lambda max is defined as the wavelength at which fluorescence emission is maximum. To determine the EC_{50}, data were fit to the agonist vs. response model in Prism 7.0d software.

GTP turnover. Where lipid environments were compared, samples were prepared as they were for fluorescence spectroscopy. Following β_2AR incubation with G protein, 1 μM GTP + 5 μM GDP mixtures (final concentration) were added to initiate the GTP turnover reaction. Reaction buffer contained 20 mM HEPES (pH 7.4) and 100 mM NaCl. Where G_{i2} and G_{i3} were compared, the GTP turnover reaction was initiated by mixing a solution containing 10 μM GTP and ligand-bound receptor (4 μM β_2AR + 800 μM epinephrine or 1 μM NTSR1 + 10 μM JMV 449) in equal volume with a solution containing 2.5 μM G protein, 20 μM GDP, 20 mM $MgCl_2$, and 200 μM TCEP. At the indicated timepoints, the GTP remaining was assessed using the GTPase-Glo assay (Promega), which detects GTP using a luminescence readout. Luminescence was detected using a SpectraMax Paradigm plate reader equipped with a TUNE SpectraMax detection cartridge (Molecular Devices). Background luminescence was subtracted from experimental reactions.

Statistics. Two-way and three-way ANOVA were performed using Graphpad Prism 7.0d.

Electrostatic modeling. Structural views and mutant models were generated using PyMOL (Schrödinger, LLC). We selected rotomer positions that most closely matched those seen in PDB 3SN6[69] (for the G_{i3}-pos. model) and PDB 1GP2[70] (for the G_s-neg. model). Continuum electrostatics models were calculated using the APBS[71] plugin (MG Lerner, University of Michigan, Ann Arbor) for PyMOL. Atomic charge and radii were calculated using the online PDB2PQR server[72] (pH 7.4, PARSE force field, hydrogen bond optimization, clash avoidance).

Nanodisc reagents. 1,2-dioleoyl-sn-glycero-3-(PE,PC,PG,PS) lipids (Avanti Polar Lipids) were used because of their low phase transition temperature. Lipids were dissolved in buffer comprised of 20 mM HEPES (pH 7.5), 100 mM NaCl, 50 mM sodium cholate, 1 mM EDTA at 16.6 mM, and were sonicated on ice before use. The MSP belt was MSP1E3D1[73]. pMSP1E3D1 was a gift from Stephen Sligar (Addgene plasmid #20066). The protein was expressed in BL21(DE3) *E. coli* (Cat. 70235-3 Millipore Sigma), and cells were lysed with sonication in 10 mM Tris-HCl, 100 mM NaH_2PO_4, 6 M GuHCl, 1% Triton X-100 (pH 8.0). The soluble fraction was isolated by centrifugation and passed through a Sepharose Fast Flow (GE Healthcare) column charged with nickel. Immobilized protein was washed with buffer comprised of 10 mM Tris-HCl, 100 mM NaH_2PO_4, 6 M GuHCl, and 0.2% Triton X-100 (pH 7.0), and then washed with buffer comprised of 50 mM NaH_2PO_4, 300 mM NaCl, and 0.2% Triton X-100 (pH 8.0). The protein was eluted using 250 mM imidazole. Impurities were precipitated by two rounds of heating at 70 °C for 1 h; after each round, the soluble fraction was isolate by centrifugation. The final soluble fraction containing MSP1E3D1 was supplemented with 20 mM sodium cholate and purified further using a HiPrep 16/60 Sephacryl S-300 HR size-exclusion column (GE Healthcare) equilibrated with buffer comprised of 20 mM HEPES, 100 mM NaCl, 1 mM EDTA, and 20 mM sodium cholate. The main peak corresponding to MSP1E3D1 was collected, dialyzed in 20 mM HEPES, 100 mM NaCl, 1 mM EDTA, 5 mM sodium cholate, concentrated to 728 μM, and frozen.

Nanodisc reconstitution. Nanodiscs were formed with one lipid type (i.e. 100% DOPS, DOPG, DOPE, or DOPC). Reconstitution was initiated by sequentially mixing water, 20× reconstitution buffer (400 mM HEPES (pH 7.5), 2 M NaCl, 20 mM EDTA), lipid, mB−β_2AR, and MSP1E3D1. The volume of mB−β_2AR stock added to the mixture was ~13% of the final mixture volume. MSP1E3D1 and mB−β_2AR were added 1:10 (molar ratio). Lipid and MSP1E3D1 were added 35:1 (molar ratio). The mixture was incubated at 4 °C for 2 h. Subsequently, Bio-Beads SM-2 resin (107.1 mg per μmol lipid, Bio-Rad) were added (4 °C for 4 h) to remove detergent, which triggers the reconstitution of mB−β_2AR in nanodisc bilayers. The soluble fraction was isolated by centrifugation. Bare nanodiscs were separated from nanodiscs containing mB−β_2AR using anti-FLAG (ATCC HB-9259) affinity chromatography. The eluate was incubated with 5 mM EDTA at 4 °C for ≥ 1.5 h to remove divalent cations. Subsequently, samples were injected into a Superdex 200 10/300GL size-exclusion column (GE Healthcare) equilibrated in buffer comprised of 20 mM HEPES (pH 7.4), 100 mM NaCl, and the main peak corresponding to nanodisc mB−β_2AR was harvested, concentrated, and frozen. The concentration of nanodisc mB−β_2AR was approximated by SDS-PAGE, using detergent solubilized β_2AR as a protein concentration reference standard.

Reporting summary. Further information on research design is available in the Nature Research Reporting Summary linked to this article.

Data availability

The source data underlying Figs. 1a, c−f, 2a, b, 3b, 4, 5a–d, and Supplementary Figs. 1a−c, 2a, b, 3a, b, 4, and 6 are provided as a Source Data File. pMSP1E3D1 is available from Addgene (#20066). All PDB files that were analyzed have been published before and can be obtained from the RCSB Protein Data Bank using the accession codes 5JQH, 3SN6, 1GP2, and 6D9H. A reporting summary for this Article is available as a Supplementary Information file. All other datasets supporting the findings of the study are available from the corresponding author on reasonable request.

Received: 4 August 2018 Accepted: 18 April 2019
Published online: 20 May 2019

References

1. Hauser, A. S., Attwood, M. M., Rask-Andersen, M., Schioth, H. B. & Gloriam, D. E. Trends in GPCR drug discovery: new agents, targets and indications. *Nat. Rev. Drug Discov.* **16**, 829–842 (2017).
2. Devic, E., Xiang, Y., Gould, D. & Kobilka, B. beta-adrenergic receptor subtype-specific signaling in cardiac myocytes from beta(1) and beta(2) adrenoceptor knockout mice. *Mol. Pharmacol.* **60**, 577–583 (2001).
3. Xiao, R. P. et al. Coupling of beta2-adrenoceptor to Gi proteins and its physiological relevance in murine cardiac myocytes. *Circ. Res.* **84**, 43–52 (1999).
4. Xiang, Y., Devic, E. & Kobilka, B. The PDZ binding motif of the beta 1 adrenergic receptor modulates receptor trafficking and signaling in cardiac myocytes. *J. Biol. Chem.* **277**, 33783–33790 (2002).
5. Xiang, Y. & Kobilka, B. The PDZ-binding motif of the 2-adrenoceptor is essential for physiologic signaling and trafficking in cardiac myocytes. *Proc. Natl Acad. Sci. USA* **100**, 10776–10781 (2003).
6. Wang, Y. et al. Norepinephrine- and epinephrine-induced distinct beta2-adrenoceptor signaling is dictated by GRK2 phosphorylation in cardiomyocytes. *J. Biol. Chem.* **283**, 1799–1807 (2008).
7. Zhu, W. Z. et al. Dual modulation of cell survival and cell death by beta(2)-adrenergic signaling in adult mouse cardiac myocytes. *Proc. Natl Acad. Sci. USA* **98**, 1607–1612 (2001).

8. Chesley, A. et al. The beta(2)-adrenergic receptor delivers an antiapoptotic signal to cardiac myocytes through G(i)-dependent coupling to phosphatidylinositol 3'-kinase. *Circ. Res.* **87**, 1172–1179 (2000).
9. Schmid, E. et al. Cardiac RKIP induces a beneficial beta-adrenoceptor-dependent positive inotropy. *Nat. Med.* **21**, 1298–1306 (2015).
10. Fajardo, G. et al. Deletion of the beta2-adrenergic receptor prevents the development of cardiomyopathy in mice. *J. Mol. Cell Cardiol.* **63**, 155–164 (2013).
11. Zamah, A. M., Delahunty, M., Luttrell, L. M. & Lefkowitz, R. J. Protein kinase A-mediated phosphorylation of the beta 2-adrenergic receptor regulates its coupling to Gs and Gi. Demonstration in a reconstituted system. *J. Biol. Chem.* **277**, 31249–31256 (2002).
12. Lefkowitz, R. J., Daaka, Y. & Luttrell, L. M. Switching of the coupling of the beta2-adrenergic receptor to different G proteins by protein kinase A. *Nature* **390**, 88–91 (1997).
13. Zhu, W. et al. Gi-biased 2AR signaling links GRK2 upregulation to heart failure. *Circ. Res.* **110**, 265–274 (2011).
14. Dawaliby, R. et al. Allosteric regulation of G protein-coupled receptor activity by phospholipids. *Nat. Chem. Biol.* **12**, 35–39 (2016).
15. Yen, H. Y. et al. PtdIns(4,5)P2 stabilizes active states of GPCRs and enhances selectivity of G-protein coupling. *Nature* **559**, 423–427 (2018).
16. Inagaki, S. et al. Modulation of the interaction between neurotensin receptor NTS1 and Gq protein by lipid. *J. Mol. Biol.* **417**, 95–111 (2012).
17. Vukoti, K., Kimura, T., Macke, L., Gawrisch, K. & Yeliseev, A. Stabilization of functional recombinant cannabinoid receptor CB(2) in detergent micelles and lipid bilayers. *PLoS ONE* **7**, e46290 (2012).
18. Kaya, A. I., Thaker, T. M., Preininger, A. M., Iverson, T. M. & Hamm, H. E. Coupling efficiency of rhodopsin and transducin in bicelles. *Biochemistry* **50**, 3193–3203 (2011).
19. Nikolaev, V. O. et al. Beta2-adrenergic receptor redistribution in heart failure changes cAMP compartmentation. *Science* **327**, 1653–1657 (2010).
20. Hong, T. & Shaw, R. M. Cardiac T-tubule microanatomy and function. *Physiol. Rev.* **97**, 227–252 (2017).
21. Houser, S. R. & Molkentin, J. D. Does contractile Ca2+control calcineurin-NFAT signaling and pathological hypertrophy in cardiac myocytes? *Sci. Signal.* **1**, pe31 (2008).
22. Verkleij, A. J. & Post, J. A. Membrane phospholipid asymmetry and signal transduction. *J. Membr. Biol.* **178**, 1–10 (2000).
23. Nygaard, R. et al. The dynamic process of beta(2)-adrenergic receptor activation. *Cell* **152**, 532–542 (2013).
24. Manglik, A. et al. Structural insights into the dynamic process of beta2-adrenergic receptor signaling. *Cell* **161**, 1101–1111 (2015).
25. Rasmussen, S. G. et al. Crystal structure of the beta2 adrenergic receptor-Gs protein complex. *Nature* **477**, 549–555 (2011).
26. Yao, X. J. et al. The effect of ligand efficacy on the formation and stability of a GPCR-G protein complex. *Proc. Natl Acad. Sci. USA* **106**, 9501–9506 (2009).
27. Shi, X. et al. Ca2+regulates T-cell receptor activation by modulating the charge property of lipids. *Nature* **493**, 111–115 (2013).
28. Crouthamel, M., Thiyagarajan, M. M., Evanko, D. S. & Wedegaertner, P. B. N-terminal polybasic motifs are required for plasma membrane localization of Galpha(s) and Galpha(q). *Cell Signal.* **20**, 1900–1910 (2008).
29. Escriba, P. V. et al. Membrane lipid therapy: modulation of the cell membrane composition and structure as a molecular base for drug discovery and new disease treatment. *Prog. Lipid Res.* **59**, 38–53 (2015).
30. Alvarez, R. et al. G protein-membrane interactions I: Galphai1 myristoyl and palmitoyl modifications in protein-lipid interactions and its implications in membrane microdomain localization. *Biochim. et Biophys. Acta* **1851**, 1511–1520 (2015).
31. Melcrova, A. et al. The complex nature of calcium cation interactions with phospholipid bilayers. *Sci. Rep.* **6**, 38035 (2016).
32. Her, C. et al. The charge properties of phospholipid nanodiscs. *Biophys. J.* **111**, 989–998 (2016).
33. Rybin, V. O., Xu, X., Lisanti, M. P. & Steinberg, S. F. Differential targeting of beta -adrenergic receptor subtypes and adenylyl cyclase to cardiomyocyte caveolae. A mechanism to functionally regulate the cAMP signaling pathway. *J. Biol. Chem.* **275**, 41447–41457 (2000).
34. Xiang, Y. Caveolar localization dictates physiologic signaling of beta 2-adrenoceptors in neonatal cardiac myocytes. *J. Biol. Chem.* **277**, 34280–34286 (2002).
35. Rosemblatt, M., Hidalgo, C., Vergara, C. & Ikemoto, N. Immunological and biochemical properties of transverse tubule membranes isolated from rabbit skeletal muscle. *J. Biol. Chem.* **256**, 8140–8148 (1981).
36. Lau, Y. H., Caswell, A. H., Brunschwig, J. P., Baerwald, R. & Garcia, M. Lipid analysis and freeze-fracture studies on isolated transverse tubules and sarcoplasmic reticulum subfractions of skeletal muscle. *J. Biol. Chem.* **254**, 540–546 (1979).
37. Pediconi, M. F., Donoso, P., Hidalgo, C. & Barrantes, F. J. Lipid composition of purified transverse tubule membranes isolated from amphibian skeletal muscle. *Biochim. et Biophys. acta* **921**, 398–404 (1987).
38. Post, J. A., Langer, G. A., Op den Kamp, J. A. & Verkleij, A. J. Phospholipid asymmetry in cardiac sarcolemma. Analysis of intact cells and 'gas-dissected' membranes. *Biochim. et Biophys. acta* **943**, 256–266 (1988).
39. Post, J. A., Verkleij, A. J. & Langer, G. A. Organization and function of sarcolemmal phospholipids in control and ischemic/reperfused cardiomyocytes. *J. Mol. Cell Cardiol.* **27**, 749–760 (1995).
40. Fearnley, C. J., Roderick, H. L. & Bootman, M. D. Calcium signaling in cardiac myocytes. *Cold Spring Harb. Perspect. Biol.* **3**, a004242 (2011).
41. Louch, W. E., Stokke, M. K., Sjaastad, I., Christensen, G. & Sejersted, O. M. No rest for the weary: diastolic calcium homeostasis in the normal and failing myocardium. *Physiology (Bethesda, MD)* **27**, 308–323 (2012).
42. Langer, G. A. & Peskoff, A. Calcium concentration and movement in the diadic cleft space of the cardiac ventricular cell. *Biophys. J.* **70**, 1169–1182 (1996).
43. Peskoff, A. & Langer, G. A. Calcium concentration and movement in the ventricular cardiac cell during an excitation-contraction cycle. *Biophys. J.* **74**, 153–174 (1998).
44. Philipson, K. D., Bers, D. M. & Nishimoto, A. Y. The role of phospholipids in the Ca2+binding of isolated cardiac sarcolemma. *J. Mol. Cell Cardiol.* **12**, 1159–1173 (1980).
45. Boettcher, J. M. et al. Atomic view of calcium-induced clustering of phosphatidylserine in mixed lipid bilayers. *Biochemistry* **50**, 2264–2273 (2011).
46. Haverstick, D. M. & Glaser, M. Visualization of Ca2+-induced phospholipid domains. *Proc. Natl Acad. Sci. USA* **84**, 4475–4479 (1987).
47. Wang, Y. H., Slochower, D. R. & Janmey, P. A. Counterion-mediated cluster formation by polyphosphoinositides. *Chem. Phys. Lipids* **182**, 38–51 (2014).
48. Zhu, W., Zeng, X., Zheng, M. & Xiao, R. P. The enigma of beta2-adrenergic receptor Gi signaling in the heart: the good, the bad, and the ugly. *Circ. Res.* **97**, 507–509 (2005).
49. Woo, A. Y., Song, Y., Xiao, R. P. & Zhu, W. Biased beta2-adrenoceptor signalling in heart failure: pathophysiology and drug discovery. *Br. J. Pharmacol.* **172**, 5444–5456 (2015).
50. Bayeva, M., Sawicki, K. T., Butler, J., Gheorghiade, M. & Ardehali, H. Molecular and cellular basis of viable dysfunctional myocardium. *Circ. Heart Fail.* **7**, 680–691 (2014).
51. Waagstein, F. & Rutherford, J. D. The evolution of the use of beta-blockers to treat heart failure: a conversation with Finn Waagstein, MD. *Circulation* **136**, 889–893 (2017).
52. Kehat, I. & Molkentin, J. D. Molecular pathways underlying cardiac remodeling during pathophysiological stimulation. *Circulation* **122**, 2727–2735 (2010).
53. Bernstein, D., Fajardo, G. & Zhao, M. The role of beta-adrenergic receptors in heart failure: differential regulation of cardiotoxicity and cardioprotection. *Prog. Pedia. Cardiol.* **31**, 35–38 (2011).
54. Xiao, R. P., Ji, X. W. & Lakatta, E. G. Functional coupling of the beta(2)-adrenoceptor to a Pertussis-toxin-sensitive G-protein in cardiac myocytes. *Mol. Pharmacol.* **47**, 322–329 (1995).
55. Sato, M., Gong, H., Terracciano, C. M., Ranu, H. & Harding, S. E. Loss of beta-adrenoceptor response in myocytes overexpressing the Na+/Ca(2+)-exchanger. *J. Mol. Cell Cardiol.* **36**, 43–48 (2004).
56. Ottolia, M., Torres, N., Bridge, J. H., Philipson, K. D. & Goldhaber, J. I. Na/Ca exchange and contraction of the heart. *J. Mol. Cell Cardiol.* **61**, 28–33 (2013).
57. Kalogeris, T., Baines, C. P., Krenz, M. & Korthuis, R. J. Cell biology of ischemia/reperfusion injury. *Int. Rev. Cell Mol. Biol.* **298**, 229–317 (2012).
58. Murphy, E. & Steenbergen, C. Ion transport and energetics during cell death and protection. *Physiology (Bethesda, MD)* **23**, 115–123 (2008).
59. Tong, H., Bernstein, D., Murphy, E. & Steenbergen, C. The role of beta-adrenergic receptor signaling in cardioprotection. *FASEB J.* **19**, 983–985 (2005).
60. Draper-Joyce, C. J. et al. 6D9H. RCSB Protein Data Bank. https://doi.org/10.2210/pdb6D9H/pdb (2018).
61. Gregorio, G. G. et al. Single-molecule analysis of ligand efficacy in beta2AR-G-protein activation. *Nature* **547**, 68–73 (2017).
62. Bohm, M. et al. Radioimmunochemical quantification of Gi alpha in right and left ventricles from patients with ischaemic and dilated cardiomyopathy and predominant left ventricular failure. *J. Mol. Cell Cardiol.* **26**, 133–149 (1994).
63. Feldman, A. M. et al. Increase of the 40,000-mol wt pertussis toxin substrate (G protein) in the failing human heart. *J. Clin. Investig.* **82**, 189–197 (1988).
64. Eschenhagen, T. et al. Increased messenger RNA level of the inhibitory G protein alpha subunit Gi alpha-2 in human end-stage heart failure. *Circ. Res.* **70**, 688–696 (1992).
65. Xiao, R. P. Enhanced Gi signaling selectively negates 2-adrenergic receptor (AR)- but not 1-AR-mediated positive inotropic effect in myocytes from failing rat hearts. *Circulation* **108**, 1633–1639 (2003).

66. Flock, T. et al. Selectivity determinants of GPCR-G-protein binding. *Nature* **545**, 317–322 (2017).
67. Conigrave, A. D. The calcium-sensing receptor and the parathyroid: past, present, future. *Front. Physiol.* **7**, 563 (2016).
68. Maeda, S. et al. Development of an antibody fragment that stabilizes GPCR/G-protein complexes. *Nat. Commun.* **9**, 3712 (2018).
69. Rasmussen, S. G. F. et al. 3SN6. RCSB Protein Data Bank. https://doi.org/10.2210/pdb3SN6/pdb (2011).
70. Wall, M. A. et al. 1GP2. RCSB Protein Data Bank. https://doi.org/10.2210/pdb1GP2/pdb (1997).
71. Baker, N. A., Sept, D., Joseph, S., Holst, M. J. & McCammon, J. A. Electrostatics of nanosystems: application to microtubules and the ribosome. *Proc. Natl Acad. Sci. USA* **98**, 10037–10041 (2001).
72. Dolinsky, T. J., Nielsen, J. E., McCammon, J. A. & Baker, N. A. PDB2PQR: an automated pipeline for the setup of Poisson-Boltzmann electrostatics calculations. *Nucleic Acids Res.* **32**, W665–W667 (2004).
73. Denisov, I. G., Baas, B. J., Grinkova, Y. V. & Sligar, S. G. Cooperativity in cytochrome P450 3A4: linkages in substrate binding, spin state, uncoupling, and product formation. *J. Biol. Chem.* **282**, 7066–7076 (2007).
74. Staus, D. P. et al. 5JQH. RCSB Protein Data Bank. https://doi.org/10.2210/pdb5JQH/pdb (2016).

Acknowledgements

We thank Betsy White for assistance with G protein and β_2AR expression, and Hideaki Kato for providing purified NTSR1. This work was supported by the National Institutes of Health grants R01NS028471 and R01GM083118 (B.K.K.). B.K.K. is supported by the Chan Zuckerberg Biohub. D.H. was supported by the German Academic Exchange Service (DAAD). M.M. was supported by the American Heart Association Postdoctoral fellowship (17POST33410958).

Author contributions

M.J.S. designed, performed, and interpreted the research, and wrote the manuscript. B.K.K. championed the investigation, advised on the project, and edited the manuscript. M.J.S. performed the β_2AR and G protein purifications, labeling, nanodisc reconstitutions, and all of the experiments, and S.M., D.H., M.M. and Y.D. provided valuable technical assistance as described: S.M. advised on cloning and provided G protein for pilot experiments. D.H. advised on G protein purification and the GTP turnover assay. M.M. advised on nanodisc reconstitution and provided MSP1E3D1 protein. Y.D. collaborated on pilot experiments not included.

Additional information

Supplementary Information accompanies this paper at https://doi.org/10.1038/s41467-019-10108-0.

Competing interests: B.K.K. is a co-founder of and consultant for ConfometRx, Inc. The other authors declare no competing interests.

Reprints and permission information is available online at http://npg.nature.com/reprintsandpermissions/

Journal peer review information: *Nature Communications* thanks Amitabha Chattopadhyay, Sergi Ferre and Anthony Lee for their contribution to the peer review of this work.

Publisher's note: Springer Nature remains neutral with regard to jurisdictional claims in published maps and institutional affiliations.